Quantum and Semiclassical Physics behind Ultrafast Optical Nonlinearity in the Midinfrared: The Role of Ionization Dynamics within the Field Half Cycle

E. E. Serebryannikov[1,2] and A. M. Zheltikov[1,2,3,*]

[1]Physics Department, International Laser Center, M.V. Lomonosov Moscow State University, Moscow 119992, Russia

[2]Russian Quantum Center, Novaya 100, Skolkovo, Moscow Region, 143025 Russia

[3]Department of Physics and Astronomy, Texas A&M University, College Station, Texas 77843-4242, USA

(Received 16 February 2014; published 25 July 2014)

Ultrafast ionization dynamics within the field half cycle is shown to be the key physical factor that controls the properties of optical nonlinearity as a function of the carrier wavelength and intensity of a driving laser field. The Schrödinger-equation analysis of a generic hydrogen quantum system reveals universal tendencies in the wavelength dependence of optical nonlinearity, shedding light on unusual properties of optical nonlinearities in the midinfrared. For high-intensity low-frequency fields, free-state electrons are shown to dominate over bound electrons in the overall nonlinear response of a quantum system. In this regime, semiclassical models are shown to offer useful insights into the physics behind optical nonlinearity.

DOI: 10.1103/PhysRevLett.113.043901 PACS numbers: 42.65.Re

Ultrafast optical science is rapidly expanding toward longer wavelengths, into the midinfrared range, opening the way toward unique regimes of interaction of high-power coherent electromagnetic radiation with matter [1,2], highly sensitive standoff detection [3], unusual filamentation scenarios [4–6], and generation of unprecedented short field waveforms on the atto- and zeptosecond time scale [7]. The latest breakthroughs in the development of mid-IR sources enabling the generation of sub-100-fs pulses with wavelengths well beyond 3 μm [8] open unique possibilities for systematic studies of optical nonlinearities in the mid-IR within a broad range of field intensities. The first experiments in this direction reveal new effects and unusual regimes of nonlinear-optical interactions [2,5], suggesting that the extension of standard models of ultrafast nonlinear-optical dynamics to the midinfrared may be nontrivial.

The main goal of this work is to shed light on unusual properties of optical nonlinearities in the mid-IR. To this end, we analyze the behavior of optical nonlinearity of a generic quantum system as a function of the wavelength of the driver field. This analysis shows that, as the wavelength of the driver is increased, free-state electrons start to dominate over bound electrons in the overall nonlinear response. In this regime, the main properties of the nonlinear response of a quantum system can be adequately understood in terms of a semiclassical nonlinear electron current modulated by the driver field.

Our analysis of the nonlinear response of an atomic system to a high-intensity laser field is based on the time-dependent Schrödinger equation (TDSE) for the wave function $\psi(\vec{r},t)$ of a hydrogen atom in the presence of a field with a Gaussian pulse shape defined by the vector potential linearly polarized along the z axis $A(t) = -E_0 f(t) \int_{-\infty}^{t} \exp[-(\tau/\tau_0)^2] \cos(\omega_0 \tau) d\tau$, where $\vec{r}$ is the radial coordinate, t is the time, and the $f(t)$ factor lets $A(t) \to 0$ at $t \to \infty$. In calculations presented below, we set $f(t)$ equal to 1 for $t < 0$ and $\exp\{-[t/(10\pi/\omega_0)]^{10}\}$ for $t > 0$. The TDSE is solved on a spatial grid using a modified fourth-order Crank-Nicholson propagator [9]. For a better convergence of the numerical procedure, the TDSE is solved in the velocity gauge. This solution is then transformed to the length gauge, yielding the $\psi(\vec{r},t)$ function used in further calculations. At the initial moment of time the quantum system is assumed to be in the $1s$ ground state of a hydrogen atom.

The length-gauge solution to the TDSE is represented as a sum $\psi(\vec{r},t) = \psi_b(\vec{r},t) + \psi_f(\vec{r},t)$ of positive- and negative-energy terms $\psi_b(\vec{r},t)$ and $\psi_f(\vec{r},t)$, corresponding to the bound and free (continuum) states of an electron [10,11]. The bound-state part of $\psi(\vec{r},t)$ can be expanded in the orthonormalized eigenfunctions $\psi_{n,l}(\vec{r})$ of the stationary counterpart of the TDSE, $\psi_b(\vec{r},t) = \sum_{n=1}^{N} \sum_{l=0}^{n-1} \alpha_{n,l}(t) \psi_{n,l}(\vec{r})$, with the probability to find an electron in a bound state with quantum numbers n and l given by $|\alpha_{n,l}|^2$, with the coefficients $\alpha_{n,l} = \int_V \psi_{n,l}(\vec{r}) \psi(\vec{r},t) d\vec{r}$ found by projecting the numerical TDSE solution $\psi(\vec{r},t)$ on the eigenfunctions of a field-free hydrogen atom. The probability to find an electron in the continuum, or population of the continuum, at the instant of time t can be found as $C(t) = \int_V |\psi_f(\vec{r},t)|^2 d\vec{r}$.

The z component of the dipole moment, $d_z(t) = \int_V e\psi^*(\vec{r},t) r \cos(\theta) \psi(\vec{r},t) d\vec{r}$, is then given by a sum of three terms, $d_z(t) = d_{\rm bb}(t) + d_{\rm ff}(t) + d_{\rm bf}(t)$, which isolate the contributions of bound-bound, free-free, and bound-free electron transitions, respectively. While the total dipole moment is gauge-invariant, the $d_{\rm bb}$, $d_{\rm ff}$, and $d_{\rm bf}$ terms are not [11]. However, as shown in an extensive literature,

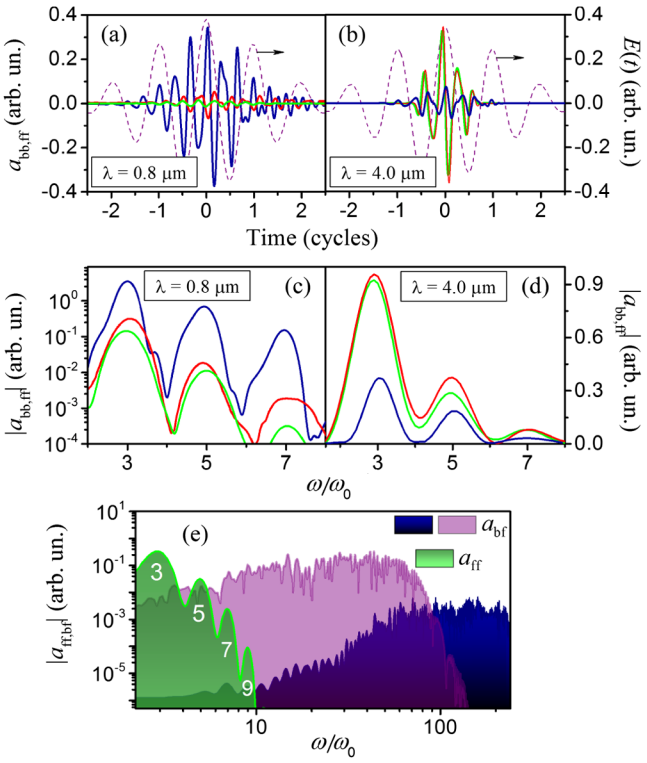

FIG. 1 (color online). Time-resolved radiation amplitudes a_{bb} (blue) and a_{ff} (red) of bound-state and free electrons (a),(b) and their spectra (c),(d) for a laser driver (purple dashed line) with $I_0 = 110$ TW/cm^2, $\tau_0 = 10/\omega_0$, and $\lambda_0 = 0.8$ (a),(c) and 4.0 μm (b),(d). Results of calculations using the semiclassical model for free electrons are given with a green line. (e) The spectra of a_{ff} (green) and a_{bf} (blue and purple) calculated using the TDSE for a laser driver pulse with $I_0 = 110$ TW/cm^2, $\tau_0 = 10/\omega_0$, and $\lambda_0 = 0.8$ (purple) and 4.0 μm (blue and green).

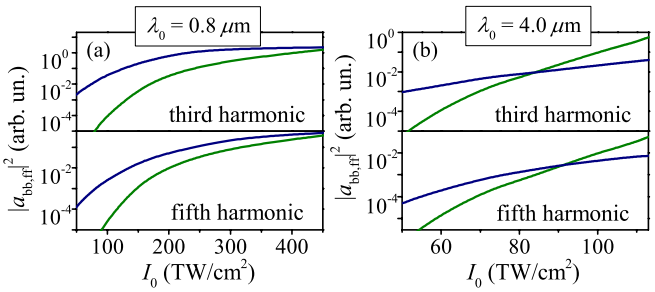

FIG. 2 (color online). Relative peak spectral intensity of the third (top box) and fifth (bottom box) harmonics generated by bound-state (blue) and free (green) electrons calculated as a function of the driver field intensity for $\lambda_0 = 0.8$ (a) and 4.0 μm (b).

including the seminar work by Lamb [12], Keldysh [13], and Corkum [14], the length gauge can be particularly helpful in offering an intuitive physical picture of a broad class of light-matter interactions. Specifically, the length-gauge analysis of the d_{bf} term has helped understand high-order harmonic generation in terms of an instructive semiclassical electron rescattering model [14,15]. Though applicable within a limited range of field intensities and frequencies [16], this model has been widely and successfully used through the past two decades in ultrafast science and attosecond technologies [17]. It will be shown below that the length-gauge analysis of the d_{ff} term can further extend a semiclassical interpretation of the nonlinear-optical response of a quantum system, helping us to understand the universal tendencies in the wavelength dependence of optical nonlinearity in terms of subcycle ionization dynamics.

In Fig. 1, we present typical time dynamics [Figs. 1(a) and 1(b)] and spectra [Figs. 1(c)–1(e)] of radiation amplitudes $a_{bb,ff,bf} \propto \partial^2 d_{bb,ff,bf}/\partial t^2$ calculated for different intensities I_0 and carrier wavelengths λ_0 of the driver field. The spectra of radiation emitted by different parts of the dipole moment are seen to exhibit strikingly different properties, reflecting significant differences in their physical nature. The intensity of low-order harmonics in the spectrum of a_{bb} [red line in Figs. 1(c) and 1(d)] rapidly decays as a function of the harmonic order, indicating that, even for relatively intense laser fields, the driver field can still be treated perturbatively for bound-state electrons, which always remain near the atomic core. The harmonic spectrum of a_{bf} sends an opposite message, as it displays an extended plateau [Fig. 1(e)], which can span over hundreds of harmonics, followed by a cutoff. These features of harmonic spectra, widely exploited in attosecond technologies [17], clearly indicate the nonpreturbative character of underlying nonlinear-optical processes [14,18].

Notably, the efficiency of high-order harmonic generation due to the a_{bf} term dramatically lowers with an increase in λ_0 [cf. the spectra in purple and blue in Fig. 1(e)], confirming the key tendencies in the wavelength scaling of high-harmonic generation revealed in the earlier studies [19,20]. As will be shown below, the spectra of low-order harmonics due to the a_{ff} term follow a radically different scaling, which makes the nonlinearity of free-state electrons a dominant part of the overall low-order nonlinear-optical response to high-intensity fields in the mid-IR. For weak fields and short λ_0, the a_{ff} term is always smaller than a_{bb} [Figs. 1(c) and 2(a)]. However, as I_0 and/or λ_0 are increased, free electrons tend to play a progressively more important role, until, eventually, in the regime of high I_0 and long λ_0, these electrons start to dominate low-order harmonic generation [Figs. 1(b), 1(d), and 2(b)].

To understand these tendencies, it is instructive to examine the buildup of the density of free electrons within the field half cycle, controlled by population of the continuum $C(t)$. For low field intensities and short driver wavelengths, the electron wave function is strongly localized around the core [Fig. 3(a)], indicating that the electrons tend to stay near the core most of the time. This correlates well with the strongly oscillatory behavior of the continuum population, seen in Figs. 4(c) and 4(d), which shows that most of the electrons that undergo ionization within a field half cycle recombine to bound states after this

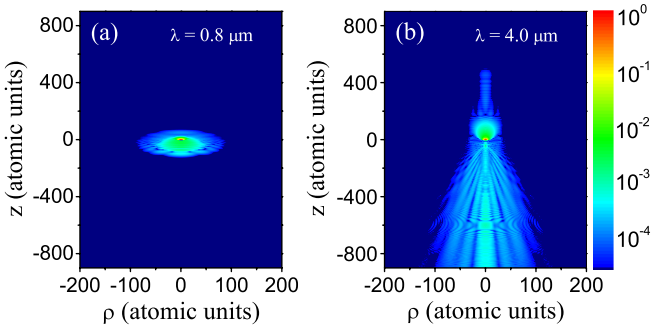

FIG. 3 (color online). The maps of the probability density $|\psi(\vec{r}, t = 0)|^2$ for a driver field with $I_0 = 110$ TW/cm^2, $\tau_0 = 10/\omega_0$, and $\lambda_0 = 0.8$ (a) and 4.0 μm (b).

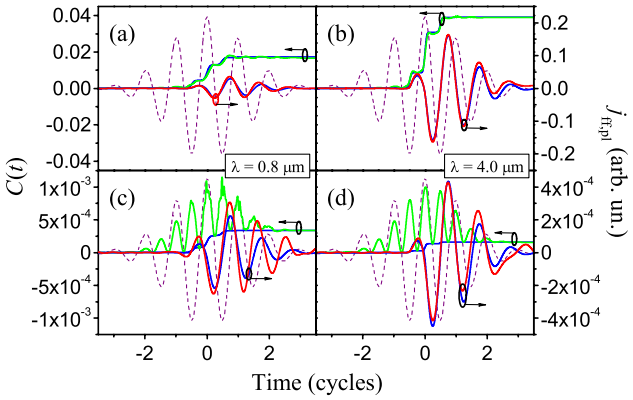

FIG. 4 (color online). Continuum population $C(t)$ calculated as a function of time using the TDSE (green), the density of free electrons calculated using the Yudin-Ivanov formula (blue), and the free-electron current density calculated using the TDSE (red) and the semiclassical model of $j_{\rm pl}$ (blue) for a driver field (dashed line) with $I_0 = 110$ (a),(b) and 50 TW/cm^2 (c),(d), $\lambda_0 = 0.8$ μm (a),(c) and $\lambda_0 = 4.0$ μm (b),(d), $\tau_0 = 10/\omega_0$.

field half cycle. Since the continuum population in this regime is low at all times [Figs. 4(c) and 4(d)], bound-state electrons dominate the nonlinear response.

For higher field I_0 and/or longer λ_0, electrons can travel further away from the core, acquiring, due to the higher field intensity and longer field cycle, a higher energy within each field half cycle. In this regime, the electron wave function is no longer tightly localized around the atomic core [Fig. 3(b)]. Since a significant fraction of electrons undergoing ionization does not recombine to bound states, the continuum population builds up in a stepwise fashion after each field half cycle, giving rise to much higher densities of free electrons in the wake of the driver pulse [Figs. 4(b) and 5(a)]. The steps in the continuum population synchronized with field half cycle translate into odd harmonics of the driver in the spectral domain [21,22]. The intensity of these harmonics is seen to be much higher than the intensity of harmonics due to bound-state electrons [Figs. 1(b) and 1(d)].

The finding that free-state electrons dominate harmonic generation in the regime of high field intensities and long carrier wavelengths suggests that some of the key properties of optical nonlinearity in this regime can be understood in terms of an appropriate semiclassical model. The length-gauge picture is instrumental in addressing this question as the canonical momentum in this gauge is equal to the kinematic momentum $\vec{p}$ and the current density does not involve the vector potential and is related to $\vec{p}$ in a straightforward way: $j_z(t) = (d/dt)[(d_z(t)] = (e\hbar/m_e)\int_V \mathrm{Im}(\psi^*(\partial/\partial z)\psi)d\vec{r} = (e/m_e)\int_V \mathrm{Re}\{\psi^* \hat{p}_z \psi\}d\vec{r} = j_{\rm bb}(t) + j_{\rm ff}(t) + j_{\rm bf}(t)$. As a semiclassical analog of the $j_{\rm ff}$ term in this expression, we examine the plasma current with the frequency-domain Fourier amplitude $j_{\rm pl}(\omega) = -(i/\omega)(e^2/m_e)\hat{F}\{E(t)n_e(t)\}$, where e is the electron charge, m_e is the electron mass, and $\hat{F}$ stands for the Fourier transform. The density of free electrons $n_e(t)$ is found from the equation $\partial n_e(t)/\partial t = W(t)[(n_0 - n_e(t)]$, where n_0 is the gas density and $W(t)$ is the ionization rate, calculated with the Yudin-Ivanov formula [23].

In the regime of high field intensities, the normalized density of free electrons $n_e(t)/n_0$ calculated with such an approach [blue curves in Figs. 4(a) and 4(b)] agrees remarkably well with the results of TDSE simulations for the continuum population [green curves in Figs. 4(a) and 4(b)]. The entire semiclassical plasma current model of $j_{\rm pl}$, on the other hand, is seen to correctly reproduce the key features in the dynamics of the free-electron current density [blue curves in Figs. 4(a) and 4(b)], providing an accurate approximation for the spectra of low-order harmonics from free-state electrons [cf. green and red lines in Fig. 1(d)]. Predictably, in the regime of low driver intensities, the semiclassical model fails to adequately reproduce TDSE simulations [Figs. 1(c) and 4(c)]. It can be also clearly seen from Figs. 4(a)–4(d) that, with λ_0 fixed, the accuracy of the semiclassical approximation increases with growing I_0. Although the I_0^N scaling with the field intensity I_0 and the number of photons required for ionization N is not applicable in the studied range of field intensities, the continuum population induced by a midinfrared driver is still a much stronger function of I_0 [cf. Figs. 4(b) and 4(d)] than the continuum population induced by a near-infrared driver [Figs. 4(a) and 4(c)].

We see from the physical arguments and examples above that ultrafast ionization dynamics, or, more specifically, the dynamics of continuum population within the field half cycle, is the key physical factor that controls the properties of the nonlinear response of a quantum system as a function of the carrier wavelength and field intensity of an optical driver. This factor can be quantified in terms of two parameters—the electron probability density transferred to the continuum by a field half cycle, i.e., $C(T/2)$, T being the field cycle, and the ratio $\xi = C(T/2)/C_{\rm max}$ of the continuum population after a field half cycle to the maximum continuum population $C_{\rm max}$ achieved within this

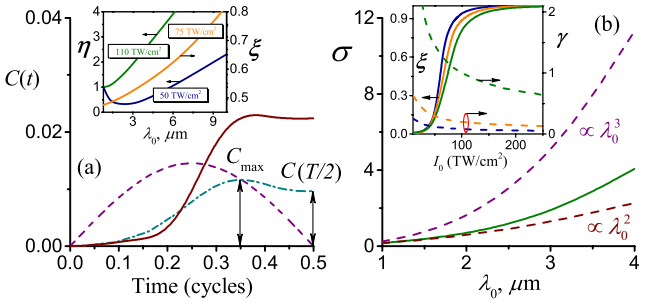

FIG. 5 (color online). (a) The continuum population as a function of time calculated within the field half cycle (dashed line) using the TDSE for $\lambda_0 = 0.8$ μm (dash-dotted line) and $\lambda_0 = 4.0$ μm (solid line) at $I_0 = 100$ TW/cm^2. The inset shows the ratio η of the continuum population after a field half cycle $C(T/2)$ for given λ_0 and I_0, normalized to $C(T/2)$ for $\lambda_0 = 0.8$ μm and the same I_0, plotted as a function of λ_0 for $I_0 = 50$ (blue line) and 110 TW/cm^2 (green line). Also shown is the ξ ratio as a function of λ_0 for $I_0 = 75$ TW/cm^2 (orange line). (b) The ratio σ calculated for $k = 1$ (third harmonic) as a function of λ_0 using the TDSE (solid green line) versus two asymptotic dependences corresponding to the ω^{-2} and ω^{-3} scaling laws (dashed lines) for $I_0 = 110$ TW/cm^2. The inset shows the Keldysh parameter γ (dashed lines) and the ratio ξ (solid lines) calculated using the TDSE as a function of the field intensity for $\lambda_0 = 0.8$ (green line), 4.0 (orange line), and 10 μm (blue line).

field half cycle [Fig. 5(a)]. Small values of ξ correspond to an oscillatory behavior of the continuum population [Figs. 4(c) and 4(d)], while $\xi \approx 1$ implies a stepwise buildup of $C(t)$ [Figs. 4(a) and 4(b)]. The ξ parameter rapidly grows with the field intensity [see inset in Fig. 5(b)], saturating at high I_0 as the fraction of free-state electrons returning to the atomic core within the field half cycle becomes vanishingly small. Below the saturation level [$I_0 < 120$ TW/cm^2 in the inset to Fig. 5(b)], ξ also rapidly grows with λ_0 [the inset in Fig. 5(a)]. Notably, the ξ parameter differs from the Keldysh parameter $\gamma = \omega_0\sqrt{(2m_eI_p)}/(eE)$ [cf. the solid and dashed lines in the inset to Fig. 5(b)], which controls the regime of photoionization.

The $C(T/2)$ parameter, as can be seen from the inset to Fig. 5(a), is a strong function of both I_0 and λ_0. For $I_0 = 110$ TW/cm^2, $C(T/2)$ in the case of a 4.0-μm driver is 3 times higher than $C(T/2)$ induced by a 0.8-μm driver [green line in the inset to Fig. 5(a)]. These much steeper steps in the buildup of continuum population in a mid-IR field [cf. Figs. 4(a) and 4(b)] translate into much more intense low-order harmonics [cf. Figs. 1(c) and 1(d)].

Using the above semiclassical picture of optical harmonic generation by free electrons and neglecting the ionization-induced depletion of the bound-state population, we represent the solution for the density of free electrons in $j_{\rm pl}$ as $n_e(t) \approx n_0 \int_{-\infty}^{t} W(\theta)d\theta$. With the driver field treated as a periodic function of time, we can expand the ionization rate, following Ref. [24], as a Fourier series $W(t) \approx W_0/2 + \sum_{k=1}^{\infty} W_k(\omega_0)\cos(2k\omega_0 t)$. Integration over time in the equation for $n_e(t)$ then yields $n_e(t) \approx (n_0W_0/2)t + \sum_{k=1}^{\infty}[n_0W_k/(2k\omega_0)]\sin(2k\omega_0 t)$. In the regime of tunneling ionization, using $W(t) \approx 4\omega_a[E_a/E(t)]\exp\{-(2E_a)/[3E(t)]\}$, where E_a is the atomic electric field unit and ω_a is the atomic frequency unit, we find $W_k \approx P(\omega_0/\pi)\exp(-3k^2/\varsigma)$, where $\varsigma = E_a/E_0$, E_0 is the amplitude of the driver field, and $P = \int_0^{\pi/\omega_0} W(t)dt$ is the probability of ionization by the field half cycle, which, in the case of tunneling ionization, is given by $P = \int_0^{\pi/\omega_0} W(t)dt = 8\sqrt{3\pi\varsigma}(\omega_a/\omega_0)\exp(-2\varsigma/3)$.

The nonlinear polarization responsible for harmonic generation by bound-state electrons is represented as $P_b(t) = \varepsilon_0\sum_{k=0}^{M}\chi^{(2k+1)}[E(t)]^{2k+1}$, where $\chi^{(2k+1)}$ is the relevant nonlinear-optical susceptibility, with the amplitude of the $(2k+1)$th harmonic given by $a_{\rm bb}^{(2k+1)} \sim \varepsilon_0\chi^{(2k+1)}\omega_0^2(E_0/2)^{2k}$. The ratio of the intensities of harmonics generated by free- and bound-state electrons is then given by $\sigma = |a_{\rm ff}^{(2k+1)}/a_{\rm bb}^{(2k+1)}| \propto 8\sqrt{3\pi\varsigma}(\omega_a/\omega_0^3)[n_0e^2 2^{2k}\exp(-3k^2/\varsigma - 2\varsigma/3)]/(m_e\varepsilon_0\chi^{(2k+1)}kE_0^{2k})$. Neglecting the wavelength dependence of the nonlinear susceptibility $\chi^{(2k+1)}$, which is weak in the case of interest, since the carrier frequency of the driver is much lower than all the electron transition frequencies in the quantum system, we find $\sigma \propto \omega_0^{-3}$.

An asymptotic ω_0^{-3} scaling is due to two multiplicative factors. The first factor is a physically significant ω_0^{-2} multiplier in the relation between $a_{\rm bb}^{(2k+1)}$ and the relevant nonlinear susceptibility, whose dependence on ω_0 is very weak because the frequencies of quantum transitions are much higher than ω_0. The second factor is the growth of P, which in the case of high field intensities scales almost linearly with the period of the driver, giving rise to an extra $1/\omega_0$ factor. For the set of parameters considered in this work, TDSE simulations yield the $\sigma(\omega_0)$ dependence [green line in Fig. 5(b)] that always fits in between ω_0^{-2} (red line) and ω_0^{-3} [purple line in Fig. 5(b)], thus verifying our qualitative physical arguments above.

To summarize, we have shown that subcycle ionization dynamics is the key physical factor that controls the properties of optical nonlinearity as a function of the carrier wavelength and intensity of a driving laser field. For high-intensity low-frequency fields, free-state electrons are shown to dominate over bound electrons in the overall nonlinear response of a quantum system. In this regime, the main properties of the nonlinear response of a quantum system can be adequately understood in terms of a semiclassical nonlinear electron current modulated by the driver field.

This research was supported in part by the Russian Foundation for Basic Research and the Welch Foundation (Grant No. A-1801). Numerical work was supported by the Russian Science Foundation (Project No. 14-12-00772). The research of E. E. S. is supported by a Russian Quantum Center fellowship.

*zheltikov@physics.msu.ru

[1] P. Agostini and L. F. DiMauro, Contemp. Phys. **49**, 179 (2008).

[2] D. Kartashov, S. Ališauskas, A. Pugžlys, A. A. Voronin, A. M. Zheltikov, and A. Baltuška, Opt. Lett. **37**, 2268 (2012).

[3] D. Kartashov, S. Ališauskas, G. Andriukaitis, A. Pugžlys, M. Shneider, A. Zheltikov, S. L. Chin, and A. Baltuška, Phys. Rev. A **86**, 033831 (2012).

[4] B. Shim, S. E. Schrauth, and A. L. Gaeta, Opt. Express **19**, 9118 (2011).

[5] D. Kartashov, S. Ališauskas, A. Pugžlys, A. Voronin, A. Zheltikov, M. Petrarca, P. Béjot, J. Kasparian, J.-P. Wolf, and A. Baltuška, Opt. Lett. **37**, 3456 (2012).

[6] L. Bergé, J. Rolle, and C. Köhler, Phys. Rev. A **88**, 023816 (2013).

[7] T. Popmintchev, M.-C. Chen, D. Popmintchev, P. Arpin, S. Brown, S. Ališauskas, G. Andriukaitis, T. Balčiunas, O. D. Mücke, A. Pugžlys, A. Baltuška, B. Shim, S. E. Schrauth, A. Gaeta, C. Hernández-García, L. Plaja, A. Becker, A. Jaron-Becker, M. M. Murnane, and H. C. Kapteyn, Science **336**, 1287 (2012).

[8] G. Andriukaitis, T. Balčiūnas, S. Ališauskas, A. Pugžlys, A. Baltuška, T. Popmintchev, M.-C. Chen, M. M. Murnane, and H. C. Kapteyn, Opt. Lett. **36**, 2755 (2011).

[9] H. Muller, Laser Phys. **9**, 138 (1999).

[10] M. Nurhuda, A. Suda, and K. Midorikawa, New J. Phys. **10**, 053006 (2008).

[11] P. Béjot, E. Cormier, E. Hertz, B. Lavorel, J. Kasparian, J.-P. Wolf, and O. Faucher, Phys. Rev. Lett. **110**, 043902 (2013).

[12] W. E. Lamb, Phys. Rev. **85**, 259 (1952).

[13] L. V. Keldysh, Sov. Phys. JETP **47**, 1945 (1964).

[14] P. B. Corkum, Phys. Rev. Lett. **71**, 1994 (1993).

[15] M. Lewenstein, P. Balcou, M. Y. Ivanov, A. L'Huillier, and P. B. Corkum, Phys. Rev. A **49**, 2117 (1994).

[16] H. R. Reiss, Phys. Rev. Lett. **101**, 043002 (2008).

[17] P. B. Corkum and F. Krausz, Nat. Phys. **3**, 381 (2007).

[18] A. B. Fedotov, S. M. Gladkov, N. I. Koroteev, and A. M. Zheltikov, J. Opt. Soc. Am. B **8**, 363 (1991).

[19] J. Tate, T. Auguste, H. G. Muller, P. Salières, P. Agostini, and L. F. DiMauro, Phys. Rev. Lett. **98**, 013901 (2007).

[20] A. D. Shiner, C. Trallero-Herrero, N. Kajumba, H.-C. Bandulet, D. Comtois, F. Légaré, M. Giguère, J.-C. Kieffer, P. B. Corkum, and D. M. Villeneuve, Phys. Rev. Lett. **103**, 073902 (2009).

[21] A. J. Verhoef, A. V. Mitrofanov, E. E. Serebryannikov, D. V. Kartashov, A. M. Zheltikov, and A. Baltuska, Phys. Rev. Lett. **104**, 163904 (2010).

[22] A. V. Mitrofanov, A. J. Verhoef, E. E. Serebryannikov, J. Lumeau, L. Glebov, A. M. Zheltikov, and A. Baltuska, Phys. Rev. Lett. **106**, 147401 (2011).

[23] G. L. Yudin and M. Y. Ivanov, Phys. Rev. A **64**, 013409 (2001).

[24] F. Brunel, J. Opt. Soc. Am. B **7**, 521 (1990).